Voltage Compensation Control and Parameter Adaptive Design of Virtual DC Machine for Microgrid Energy Storage Converters

Hailiang XU, Honglong ZHANG, Pingjuan GE, and Cong WANG

***Abstract*—To enhance the stability of a DC microgrid, a promising approach is to control the energy storage converter via the virtual DC machine control (VDMC), which can improve inertia and damping of the system. However, the conventional VDMC suffers from poor dynamic performance during large disturbances, partially due to its fixed control parameters. To track such problem, this paper proposes a voltage compensation control and parameter adaptive method for the VDMC of microgrid energy storage converters. Firstly, the dynamic process of microgrid bus voltage under disturbance is analyzed, and an armature voltage compensation control loop is then constructed. Subsequently, the influences of inertia, damping and compensation coefficients on the system dynamic characteristics are evaluated, and a parameter adaptive control method for the improved VDMC is proposed. Simulation and experimental results demonstrate that the proposed control strategy can effectively mitigate the DC bus voltage fluctuations, with faster response and smaller overshoot than the conventional VDMC strategy.**

***Index Terms*—Adaptive parameters control, armature voltage compensation, DC microgrid, energy storage converters, virtual DC machine control.**

I. Introduction

DC microgrid have received a lot of attention in recent years due to the absence of frequency and reactive power problems [1]–[5]. In a DC microgrid, the power flow of the distributed power sources, energy storage, loads and other devices all need to interact through the DC bus. Hence, the stability of the DC bus voltage becomes an important indicator to judge the stability of a DC microgrid [6], [7]. However, some distributed power sources, such as wind power and photovoltaic, may have negative impact on grid stability due to their fluctuating and intermittent nature. At the same time, the DC microgrid system lacks inertia and damping [8]. In the event of large disturbances, the DC bus voltage may change suddenly. This can be detrimental to the stability of DC microgrid systems. Therefore, it is an urgent problem for DC microgrid to suppress voltage fluctuations [6]–[8].

It is noteworthy that, the energy storage converters can smooth out the power fluctuations due to their energy regulation capacity [9]–[11]. Several studies have been conducted to enhance the bus voltage stability of DC microgrid by optimizing the control of energy storage converters. The traditional dual closed-loop voltage and current regulation method utilizing a proportional-integral controller can partially stabilize the bus voltage. However, since it is inadequate to provide sufficient inertia and damping, the bus voltage would fluctuate severely during inrush load disturbances [12], [13]. In [14] and [15], the DC bus receives additional inertia support by introducing virtual capacitors into the energy storage converter. Based on this, a flexible virtual inertia control strategy is proposed in [16], where the virtual capacitor can be adapted to changes in the rate of DC bus voltage. However, measuring the rate of DC bus voltage change requires low-pass filtering and multiple steps. Additionally, the impact of the virtual capacitance change rate on control stability is usually ignored. In [17]–[21], the mathematical model of a DC machine is equivalently analogous to an energy storage converter, and a virtual DC machine control (VDMC) method is proposed. With this method, the damping and inertia characteristics are introduced into the energy storage converter, which improves the stability of the DC microgrid to a certain extent.

The aforementioned VDMC strategies offer increased inertia and damping to the DC microgrid, thus partially resolving the issue of insufficient inertia and damping. Nevertheless, existing control methods struggle to effectively manage the bus voltage fluctuations during significant disturbances. In addition, the traditional VDMC parameters remain constant and cannot adjust according to the dynamic process of the DC bus, making it challenging to achieve ideal dynamic regulation performance [22].

To address such issues, an improved control strategy for the microgrid energy storage converters is proposed. And the specific contributions can be summarized as follows:

1) The analysis of bus voltage dynamic process during large disturbances is conducted, and an armature voltage compensa-

Manuscript received July 6, 2023; revised September 6, 2023; accepted October 8, 2023. Date of publication March 30, 2024; date of current version October 13, 2023. This work was supported by the National Natural Science Foundation of China under Grant 52077222, and the Shandong Provincial Natural Science Foundation under Grant ZR2020ME202. *(Corresponding authors: Pingjuan Ge.)*

All authors are with China University of Petroleum (East China), Qingdao 266580, Shandong, China (e-mail: xuhl@upc.edu.cn; zhl_upc@163.com; gepingjuan@upc.edu.cn; wcwcupc@163.com).

Digital Object Identifier 10.24295/CPSSTPEA.2023.00045

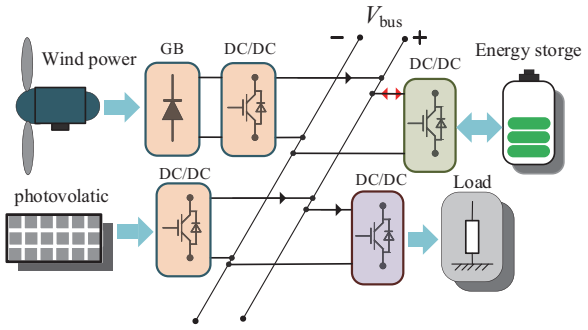

Fig. 1. The structure of a DC microgrid.

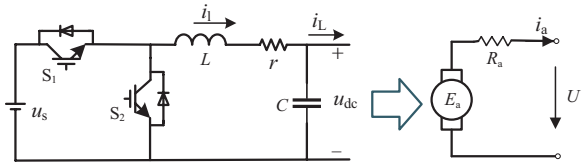

Fig. 2. Virtual DC machine model.

tion control loop is implemented.

2) The influence of inertia, damping and compensation coefficients on the voltage dynamic characteristics are evaluated. Then, a parameter adaptive control strategy is proposed.

The rest of the paper is organized as follows: In Section II, the traditional VDMC is added with armature voltage compensation control and the modeling analysis is carried out. By analyzing the influence of each parameter on the dynamic process, a new adaptive control method is proposed and the parameters are designed in Section III. The simulation and experimental results are performed to verify the design in Section IV. Some conclusions are finally drawn in the final section.

II. The Armature Voltage Compensation Based VDMC

A. The Conventional VDMC

Fig. 1 depicts the structure of a DC microgrid, featuring various distributed generation devices such as photovoltaics and wind turbines, energy storage devices, and load devices. Each component is linked to the DC bus through converters.

When the energy storage converter is controlled by VDMC, the topology of the energy storage converter and its equivalent DC machine model are shown in Fig. 2 [16], [22], [23], where u_s is the input voltage of the energy storage converter; i_l is the current flowing through an inductor; i_L is the output current; u_{dc} is the output voltage; i.e., the DC bus voltage; L, C are the inductor and capacitor respectively; S_1, S_2 are the switching tubes; E_a is the equivalent DC machine armature potential; i_a is the equivalent DC machine armature current; R_a is the equivalent resistance of the armature circuit.

Referring to Fig. 2, the armature circuit equation of the DC machine at steady state can be obtained as:

$$u_{dc} = u_{dc0} = E_a - i_a R_a \tag{1}$$

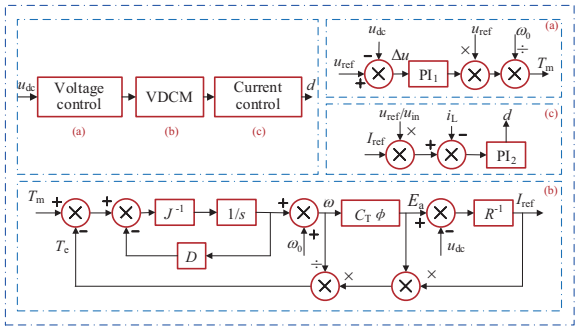

Fig. 3. The control loops of VDMC.

where u_{dc0} is the steady state voltage; $E_a = C_T\phi\omega$ is the armature voltage; C_T is the torque coefficient; ϕ is the flux per pole and ω is the actual mechanical angular velocity of the DC motor.

The rotor motion equation of a DC machine can be expressed as:

$$T_m - T_e = J\frac{d\omega}{dt} + D(\omega - \omega_0) \tag{2}$$

where T_m and T_e are the mechanical torque and electromagnetic torque of the DC machine respectively; J is the rotational inertia; D is the damping factor; ω_0 is the rated mechanical angular speed of the DC machine.

The electromagnetic torque of the DC machine T_e is:

$$T_e = \frac{P_e}{\omega} \tag{3}$$

where P_e is the electromagnetic power.

From (1)–(3), the VDMC block diagram for a conventional energy storage converter can be depicted as Fig. 3.

By integrating the aforementioned insights and Fig. 2, when the load is disturbed, the output voltage can be expressed as:

$$u_{dc} = u_{dc0} + \Delta u_{dc} = E_a - (i_a + \Delta i_a)R_a \tag{4}$$

where Δu_{dc}, Δi_a denote the DC bus voltage and current disturbances respectively.

From (1) and (4), the value of the DC bus voltage disturbance can be obtained as:

$$\Delta u_{dc} = -\Delta i_a R_a \tag{5}$$

From (5), it can be observed that since the DC bus capacitance is finite, sudden load surges can cause instantaneous increase in the current. Consequently, the fluctuations in the DC bus voltage disturbance, represented by Δu_{dc}, may endanger the overall stability of the DC microgrid system.

B. The Proposed VDMC

To mitigate the undesirable DC bus voltage fluctuations, a possible solution is to introduce a compensation link for

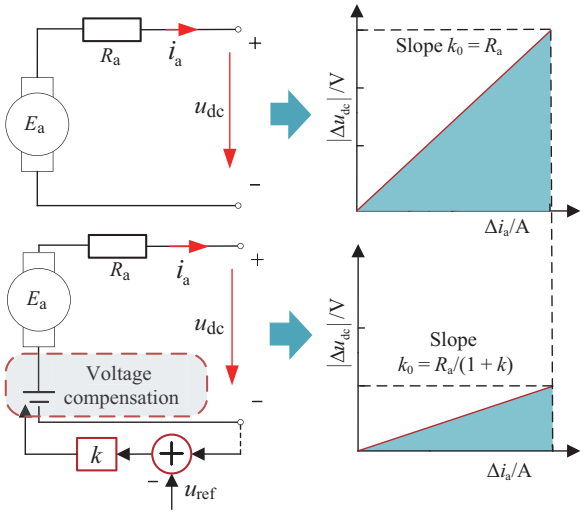

Fig. 4. Disturbance diagram of voltage and current.

the armature voltage E_a, as shown in the equivalent model depicted in Fig. 3. Specifically, when the DC bus voltage drops, the armature voltage E_a can be raised suitably to counterbalance the voltage change. Conversely, if the DC bus voltage increases, the armature voltage can correspondingly get lowered. The compensation mechanism should fulfill two conditions:

1) The armature voltage compensation should be zero at steady state.

2) The armature voltage compensation needs to adjust dynamically in response to the voltage disturbances.

Based on these requirements, the disturbance value Δu_{dc} of the DC bus voltage can be used directly as a compensation to the armature voltage to suppress fluctuations in the DC bus voltage.

Once the armature voltage is compensated, the steady output voltage can be expressed as:

$$u_{dc} = u_{dc0} = E_a - i_a R_a \tag{6}$$

Thereupon, when the load is disturbed, the output voltage can be written as:

$$u_{dc} = u_{dc0} + \Delta u_{dc} = E_a - k\Delta u_{dc} - (i_a + \Delta i_a)R_a \tag{7}$$

Combining (6) and (7), the DC bus can be expressed as:

$$\Delta u_{dc} = -\Delta i_a R_a / (1+k) \tag{8}$$

Referring to (8), it reveals that, during a load disturbance in the DC microgrid, the voltage disturbance magnitude for the enhanced VDMC is only $1/(1 + k)$ of that in the conventional one, as depicted in Fig. 4. Hence, the energy storage converter can achieve more mitigation of DC bus voltage fluctuations.

Accordingly, the improved VDMC block diagram can be obtained as Fig. 5.

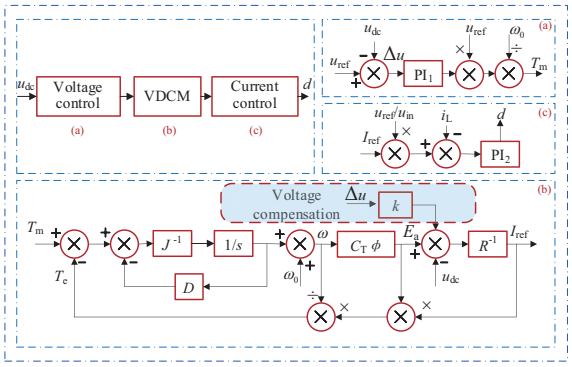

Fig. 5. Control loops of the improved VDMC.

C. Dynamic Response Analysis

To evaluate the influence of control parameters on the improved VDMC, the small-signal modelling approach is adopted. Based on Fig. 2 and (1)–(3), the small-signal model of the converter can be expressed in Fig. 6. $G_M(s)$ represents the transfer function of pulse width modulation (PWM), and $G_1(s)$, $G_2(s)$, $G_3(s)$, and $G_4(s)$ are defined as:

$$G_1(s) = \frac{u_{ref} G_{PI1}(s)}{\omega_0} \tag{9}$$

$$G_2(s) = \frac{C_T\phi}{Js + D} \tag{10}$$

$$G_3(s) = G_{PI2}(s)G_M(s) \tag{11}$$

$$G_4(s) = G_1(s)G_2(s) + k \tag{12}$$

where $G_{PI1}(s) = k_{pu} + k_{iu}/s$ and $G_{PI2}(s) = k_{pi} + k_{ii}/s$ represent the PI controllers of the voltage and current control loop, respectively.

Therefore, as shown in Fig. 6, the closed-loop transfer function between Δu_{dc} and Δu_{ref} as well as the transfer function from Δu_{dc} to the disturbance current Δi_L can be expressed as (13) and (14), respectively.

$$G_u(s) = \frac{\Delta u_{dc}}{\Delta u_{ref}} = \frac{H_1(s)H_2(s)}{1 + H_1(s)H_2(s)H_3(s)} \tag{13}$$

$$G_z(s) = \frac{\Delta u_{dc}}{\Delta i_L} = \frac{-H_2(s)}{1 + H_1(s)H_2(s)H_3(s)} \tag{14}$$

$$H_1(s) = \frac{[k + G_1(s)G_2(s)]G_3(s)}{[G_2(s)C_T\phi + R_a][Ls + r + G_3(s)]} \tag{15}$$

$$H_2(s) = \frac{1}{Cs} \tag{16}$$

$$H_3(s) = \frac{G_2(s)C_T\phi + R_a}{[k + G_1(s)G_2(s)]G_3(s)} + \frac{1}{k + G_1(s)G_2(s)} + 1 \tag{17}$$

The dynamic behavior of the improved VDMC system depends on its parameter values, i.e., J, D, and k. Hence, tuning

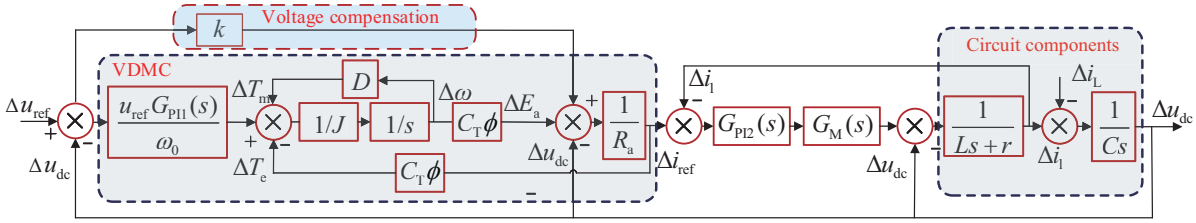

Fig. 6. Small signal model of improved VDCM control.

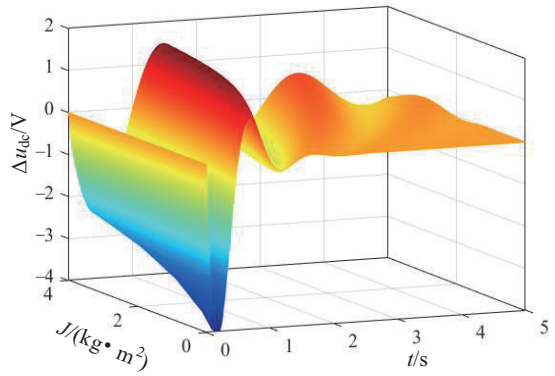

(a)

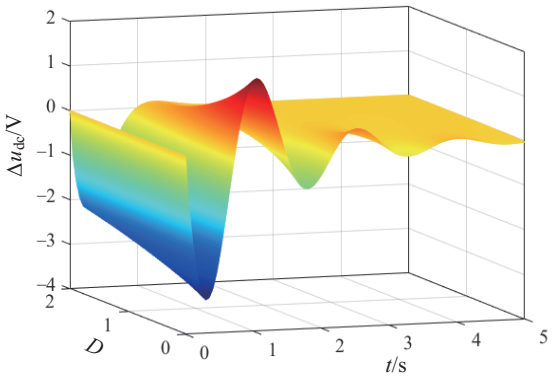

(b)

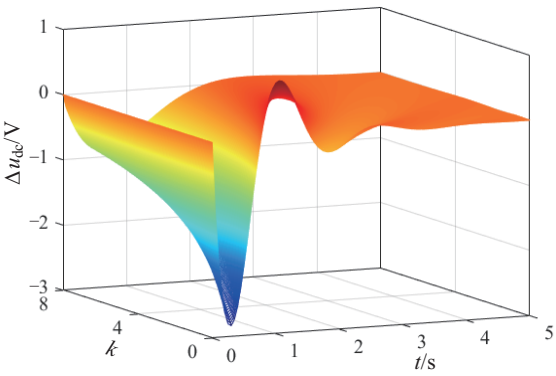

(c)

Fig. 7. Output impedance unit step response when the control parameter changes. (a) Unit step response for a J change. (b) Unit step response for a D change. (c) Unit step response for a k change.

these parameters plays a critical role in optimizing the dynamic performance of the system.

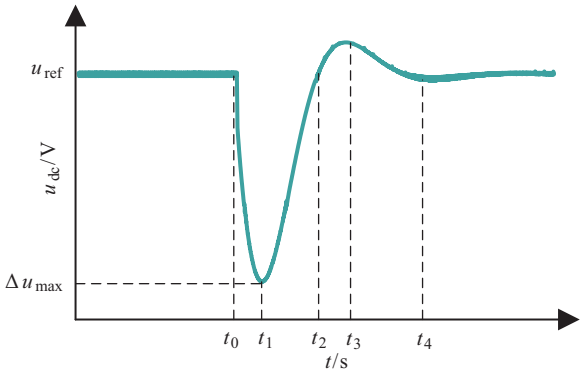

Fig. 8. The DC bus voltage dynamic response.

Based on the closed-loop transfer function of (14), the unit step response of the output impedance $G_z(s)$ with varying control parameters can be obtained, as illustrated in Fig. 7. It can be observed that, as the inertia J increases, the voltage response becomes slower, and the voltage fluctuations become smaller. This indicates that a higher inertia can improve the system's ability to suppress voltage changes, but it will also result in increased voltage overshoot and longer dynamic time. Conversely, within a certain range, as the damping factor D increases, the voltage overshoot reduces significantly, and the time for the system to recover stability is shorter. Moreover, an increase in the compensation factor k can mitigate the amplitude of DC bus voltage disturbance and voltage overshoot effectively. However, it comes at the expense of a long time for the system to recover stability.

To summarize, the dynamic characteristics of the system are greatly impacted by the control parameters. Thus, optimizing these parameters would significantly enhance the system's performance.

III. Parameter Adaptive Approach of the Proposed VDMC

A. Parameter Adaptive Method

As the control parameters of traditional VDMC strategies are typically unchanged, it is not practical to make real-time adjustments to achieve optimal dynamic regulation performance. To tackle this issue, a parameter adaptive control method is proposed in this section.

Taking the load power surge as an example, the typical waveform of the DC bus voltage can be divided into five stages, as shown in Fig. 8. The DC bus voltage operates steadily from phase 0 to t_0; from t_0 to t_1, the DC bus voltage starts to

TABLE I
THE PARAMETER ADJUSTMENT PROCESS

Stage	$\|\Delta u\|$	$\Delta u(\mathrm{d}u/\mathrm{d}t)$	J	D	k
0–t_0	$\|\Delta u\|<u_{\lim}$	0	J_0	D_0	k_0
t_0–t_1	$\|\Delta u\|\geqslant u_{\lim}$	$\Delta u(\mathrm{d}u/\mathrm{d}t)>0$	+	+	+
t_1–t_2	$\|\Delta u\|\geqslant u_{\lim}$	$\Delta u(\mathrm{d}u/\mathrm{d}t)<0$	−	+	−
t_2–t_3	$\|\Delta u\|\geqslant u_{\lim}$	$\Delta u(\mathrm{d}u/\mathrm{d}t)>0$	+	+	+
t_3–t_4	$\|\Delta u\|\geqslant u_{\lim}$	$\Delta u(\mathrm{d}u/\mathrm{d}t)<0$	−	+	−

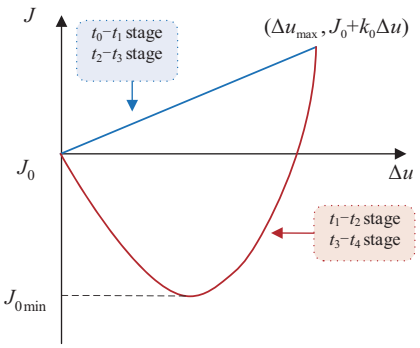

Fig. 9. Diagram of parameter adaptive control.

fluctuate down until it drops to the maximum disturbance voltage, i.e., $\Delta u_{\max}$. According to the above analysis, a larger J, D and k can be used at this time to suppress the fluctuation of the DC bus voltage, slowing down the rate of voltage change. From t_1 to t_2 stage, the DC bus voltage starts to recover from the maximum disturbance voltage to the steady state. Herein, a smaller J and k should be used to speed up the system recovery, while increasing D to reduce the overshoot. From t_2 to t_3, the bus voltage overshoot and deviation from the steady state value that is similar to that in the t_0 to t_1 stage, and a larger J, D and k should be used. From t_3 to t_4, the bus voltage recovers from the deviation value to the steady state one, which is similar to that in the t_1 to t_2 stage. In this stage, a smaller J and k should be used to reduce the voltage recovery time. The regulating process can be summarized in Table I.

To optimize the dynamic process by adjusting parameters, an improved dynamic process is designed, as shown in Fig. 9. During the period when the voltage dips, the parameters of J and k gradually get increased according to a first-order function to reduce voltage fluctuations. During the voltage recovery period, J and k get decreased according to a second-order function. Similarly, the damping coefficient D only needs to increase according to a first-order function.

Accordingly, the tuning principle of J, D and k of the improved VDMC can be expressed as (18)–(20). Since the adaptive process for J and k is the same, only the adaptive process of J is presented here.

From Table I and Fig. 9, the principle for the values of J, D and k in VDCM parameter adaptive control can be expressed as:

$$J=\begin{cases} J_0 & |\Delta u|<u_{\lim} \\ J_0+h_1|\Delta u| & |\Delta u|\geqslant u_{\lim} \text{ and } \Delta u\dfrac{\mathrm{d}u}{\mathrm{d}t}\geqslant 0 \\ a_1(|\Delta u|-b_1)^2+J_{0\min} & |\Delta u|\geqslant u_{\lim} \text{ and } \Delta u\dfrac{\mathrm{d}u}{\mathrm{d}t}<0 \end{cases} \tag{18}$$

$$D=\begin{cases} D_0 & |\Delta u|<u_{\lim} \\ D_0+h_2|\Delta u| & |\Delta u|\geqslant u_{\lim} \end{cases} \tag{19}$$

$$k=\begin{cases} k_0 & |\Delta u|<u_{\lim} \\ k_0+h_3|\Delta u| & |\Delta u|\geqslant u_{\lim} \text{ and } \Delta u\dfrac{\mathrm{d}u}{\mathrm{d}t}\geqslant 0 \\ a_3(|\Delta u|-b_3)^2+k_{0\min} & |\Delta u|\geqslant u_{\lim} \text{ and } \Delta u\dfrac{\mathrm{d}u}{\mathrm{d}t}<0 \end{cases} \tag{20}$$

where $a_1=h_1/(\Delta u_{\max}-2b_1)$, $b_1=-c_1+\sqrt{c_1^2+h_1c_1\Delta u_{\max}}/h_1$, $c_1=J_0-J_{0\min}$; $a_3=h_3/(\Delta u_{\max}-2b_3)$, $b_3=-c_3+\sqrt{c_3^2+h_3c_3\Delta u_{\max}}/h_3$, $c_3=k_0-k_{0\min}$.

In (18)–(20), J_0, D_0 and k_0 denote the initial values of the inertia, damping and compensation factors, respectively; h_1 and h_2 are the amplification factors for the inertia J and damping D factor, respectively, while h_3 is the amplification factor for the compensation factor k; Δu is the DC bus deviation value; $u_{\lim}$ is the bus voltage difference threshold to determine whether the DC bus voltage fluctuates. $J_{0\min}$ is the minimum value for the inertia parameter.

B. Parameter Tunings

To ensure optimal dynamic performance, it is crucial to conduct a comprehensive analysis of the dynamic response for the selected VDCM parameters. The closed-loop dominant pole diagrams are plotted with the parameters of J ranging from 0.05 to 2, D varying from 0.2 to 5, and k varying from 0 to 5, as illustrated in Fig. 10.

As show in Fig. 10(a), as the inertia increases, a set of conjugate poles gradually approach the origin. It implies that the response speed of the enhanced VDMC system slows down, leading to a higher overshoot and longer response time.

In Fig. 10(b), it can be seen that as the damping coefficient increases, a pair of conjugate poles gradually approach the imaginary axis. This suggests that an increase in system damping will result in a reduction of overshoot. Therefore, if D is too small, it will lead to reduced system stability. However, if D is too large, the system damping will become excessive, resulting in longer dynamic time.

Fig. 10(c) illustrates that as the compensation coefficient increases; a pair of conjugate poles approach both the imaginary axis and the origin. This indicates that the system damping would get increased, resulting in a decrease in overshoot and a reduction in the control system's response speed. These findings are consistent with the dynamic analysis results aforementioned.

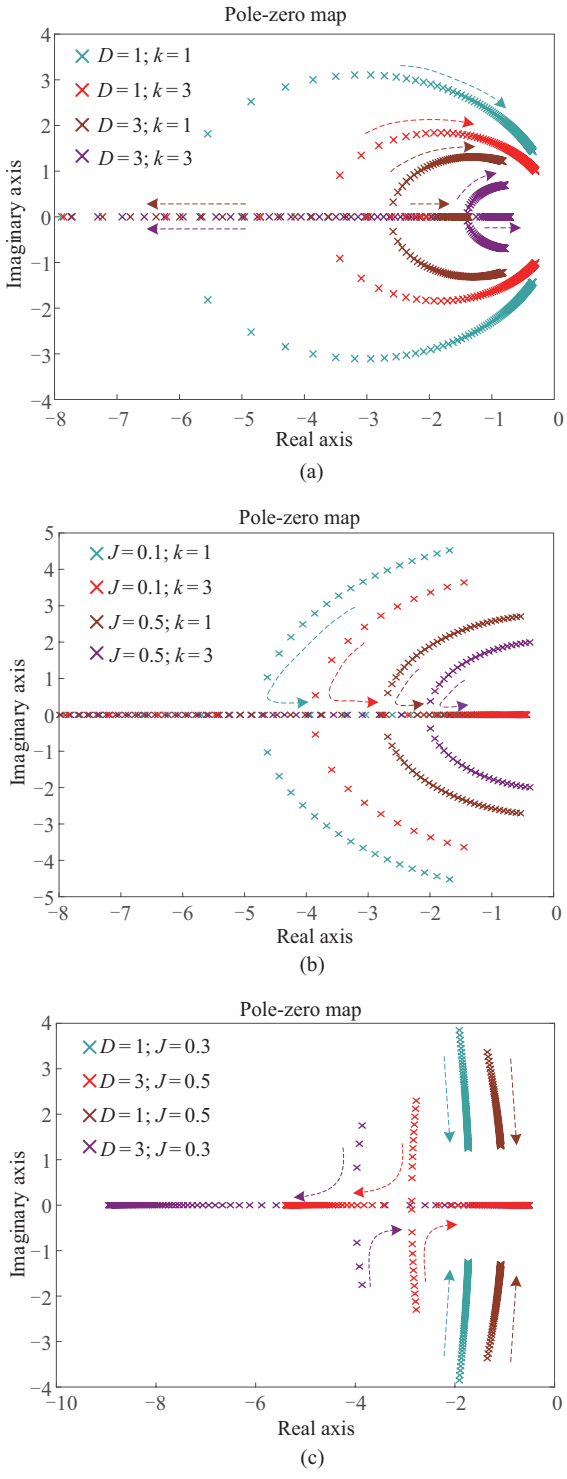

Fig. 10. Close loop pole map when the control parameter changes. (a) Varied J, (b) Varied D and (c) Varied k.

To ensure safety, it is necessary to consider the influence of parameters on both system stability and step response characteristics in a comprehensive manner. In a pole-zero plot, if the poles are too close to the imaginary axis, it can lead to slow system response and if the poles are too close to the real axis, it can decrease the stability of the system. As a result, the parameters of J and D are set to make the phase margin be within the range 20°−70°, while the steady state value is set to obtain a phase margin of 40°−50°. Specifically, J is taken as 0.1−1 and J_0 is taken as 0.3; D_0 is set as 2. From the pole-zero plot, it can be seen that stability gets maintained with the k ranging from 0 to 5. However, if k is too large, the system's dynamic time becomes too long. Therefore, it is recommended to set the value of k between 0 and 3.

TABLE II
SIMULATION PARAMETERS

Parameters	Value
Inductance L_1/mH	1
Line resistance r_1/Ω	0.045
Bus capacitance C_1/μF	470
Input voltage u_s/V	50
Rated DC bus voltage u_{ref}/V	30
Moment of inertia J_0/(kg·m^2)	0.3
Damping coefficient D_0	2
Compensation factor k_0	2
Electromotive force coefficient $C_T\Phi$/(N·m/A)	3
Equivalent resistance of armature loop R_a/Ω	0.5

The stability of DC bus voltage is a critical aspect for the normal operation of a DC microgrid. The bus voltage should be within a specific range during system disturbances [24]. In this paper, the allowed change range is set to be 10% of the steady-state value, i.e., the maximum disturbance voltage, denoted by Δu_{max}. By substituting this value into (19) and (20), and maintaining a certain margin of safety, it comes out that $h_1 = 0.2$ and $h_3 = 0.2$.

IV. Simulation and Experimental Verification

A. Simulation Studies

To verify the effectiveness of the proposed control strategy, a simulation model of the DC microgrid was built in the MATLAB/Simulink with the parameters shown in Table II. The influence of parameters on the dynamic characteristics is verified, as shown in Fig. 11. It can be observed that increasing the J will reduce voltage fluctuation, but increase overshoot. Increasing the damping coefficient D slightly, will reduce the voltage fluctuation and overshoot, but excessive damping will lead to extended dynamic time. With an increase in compensation coefficient k, the voltage fluctuation and overshoot can be effectively reduced, but the corresponding dynamic time is still prolonged. It can be seen that the above conclusions are consistent with those obtained through Fig. 7.

As depicted in Fig. 12, the initial value of the DC bus voltage is 30 V, so the ΔU_{max} is selected to be 10% of the steady state value, i.e., 3 V. A sudden increase in load power from 30 W to 120 W occurs at 8 s, then the power dropped from 120 W to 70 W at 12 s. Compared with the conventional VDMC, the peak DC bus voltage fluctuation with the proposed control gets

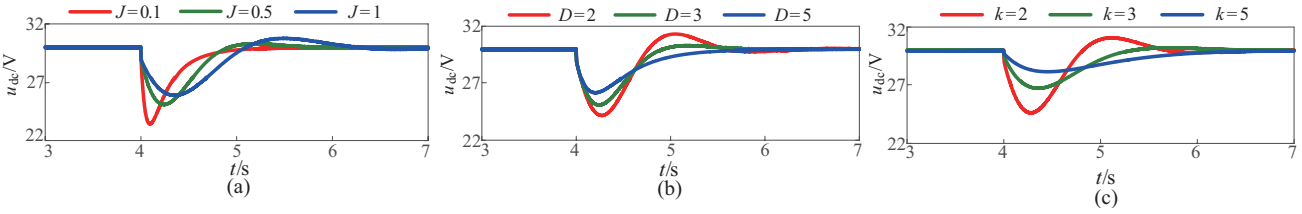

Fig. 11. Simulation waveforms of the influence of parameters on the dynamic characteristics different control strategies during load power changes from 30 W to 90 W. (a) Inertia J changes. (b) Damping D changes. (c) Compensation coefficient k changes.

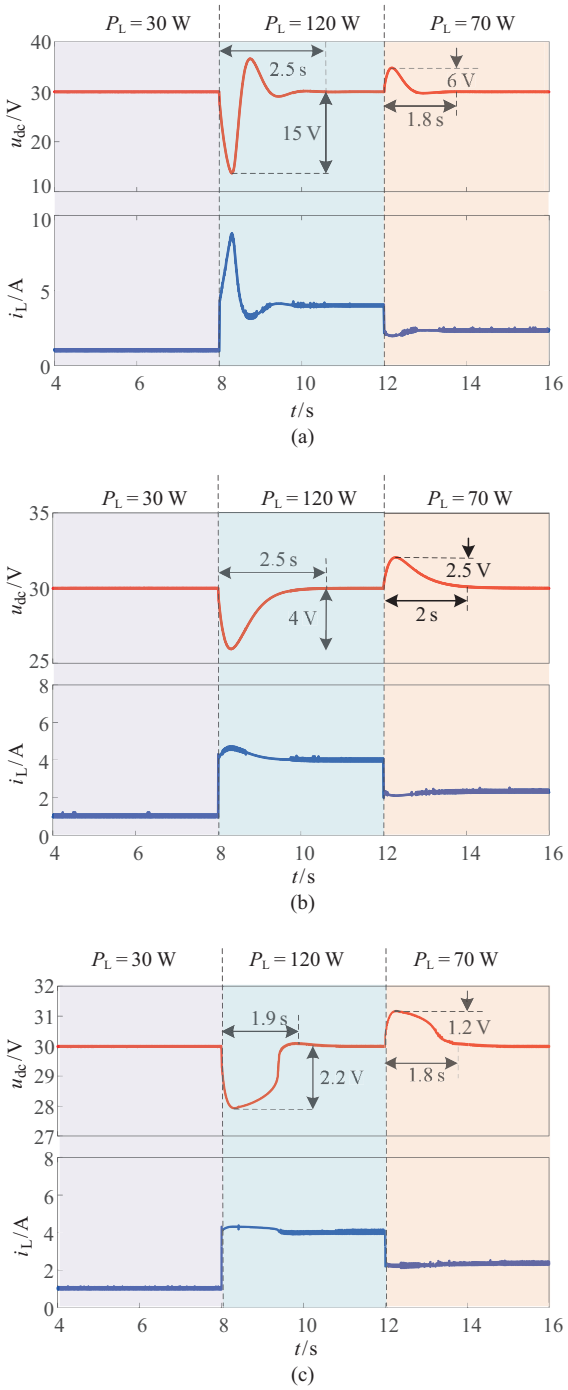

Fig. 12. Simulation waveforms of different control strategies. (a) The traditional VDMC. (b) The VDMC with armature voltage compensation. (c) The adaptive control.

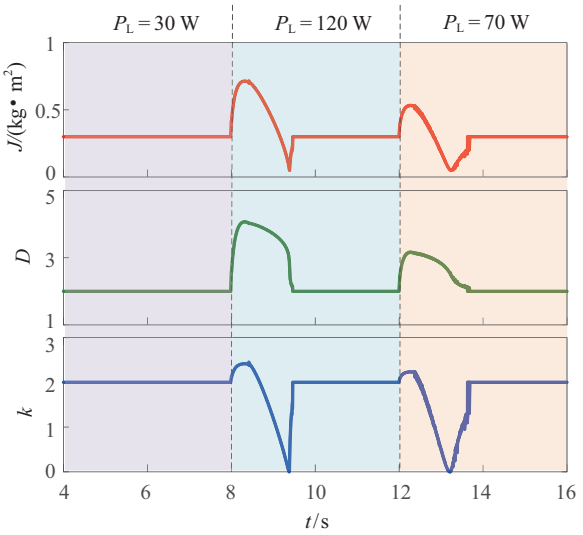

Fig. 13. The adaptive variation process diagram of J, D, and k.

reduced from approximately 15 V to 4 V, with the dynamic response time keeps unchanged. Besides, the bus voltage fluctuation is reduced from approximately 6 V to 2.5 V, with the dynamic response time extended from 1.8 s to 2 s when the power dropped. In contrast, the improved adaptive control can effectively reduce the peak DC bus voltage fluctuation to 2.2 V and the dynamic response time to 1.9 s when the power increased. At the same time, the improved adaptive control also can reduces the peak DC bus voltage fluctuation to 1.2 V and the dynamic response time to 1.8 s when the power dropped. Hence, the improved adaptive control strategy can significantly enhance the stability of the DC microgrid.

Fig. 13 shows the variation of J, D, and k during the adaptive process. It can be seen that when the voltage deviates from its steady-state value, the virtual inertia (J), damping coefficient (D), and compensation coefficient (k) will all increase. This can effectively reduce voltage fluctuations. During the recovery stage, the value of J, D, and k are gradually decrease, but D is only decrease to its steady-state value D_0. Meanwhile, J and k continue to decrease, the voltage recovery rate is accelerated, the system's dynamic response time is shortened, and the absence of any control parameter mutation during the adaptive process ensures system stability.

B. Experimental Verification

To further validate the effectiveness of the proposed control

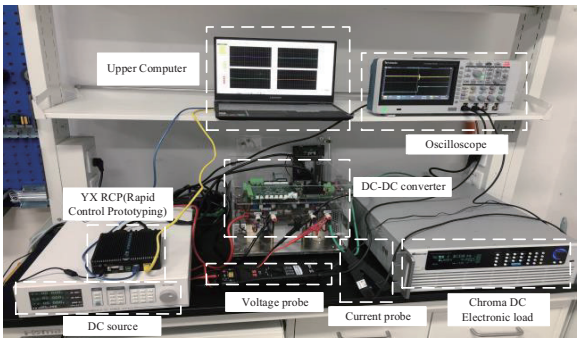

Fig. 14. The experimental setup.

TABLE III
EXPERIMENTAL SYSTEM PARAMETERS

Parameters	Value
Inductance L_1/mH	1
Line resistance r_1/Ω	0.045
Bus capacitance C_1/μF	470
Input voltage u_s/V	70
Rated DC bus voltage u_{ref}/V	50
Moment of inertia J_0/(kg·m^2)	0.3
Damping coefficient D_0	2
Compensation factor k_0	2
Electromotive force coefficient $C_T\Phi$/(N·m/A)	3
Equivalent resistance of armature loop R_a/Ω	0.5

strategy, a test platform was established in the laboratory, as depicted in Fig. 14, with the parameters shown in Table III. The experimental setup encompasses a programmable DC source, a DC electronic load, a DC/DC converter, a rapid control prototyping unit, an upper computer, an oscilloscope, and a probe. During the experiment, the input voltage is maintained at 70 V, while the output voltage command of the converter is set to 50 V. Then Δu_{max} is selected to be 10% of the steady state value, i.e., 5 V.

Fig. 15 displays the output voltage and current waveforms under different control methods during a sudden change in load power. The results reveal that the traditional VDMC approach results in a peak fluctuation of 7 V (14% of the steady state value of the bus voltage), with a DC bus voltage recovery time of 1.2 s. When the armature voltage compensation is added, the voltage fluctuation is about 2 V (4% of the steady state value), and the dynamic time is about 1.2 s. The DC bus voltage fluctuation is much less than the traditional VDMC control, but the dynamic time is not reduced effectively. Contrastively, with the proposed adaptive control, the voltage is further reduced to around 1 V (2% of the steady state value), the dynamic time can be reduced significantly to around 0.4 s.

Based on the experimental findings, it can be inferred that the improved adaptive control method is highly proficient in suppressing DC bus voltage fluctuations during significant disturbances.

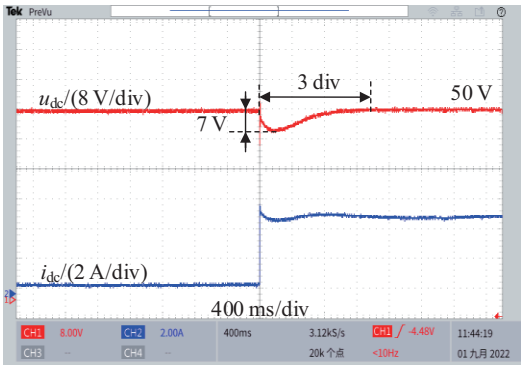

(a)

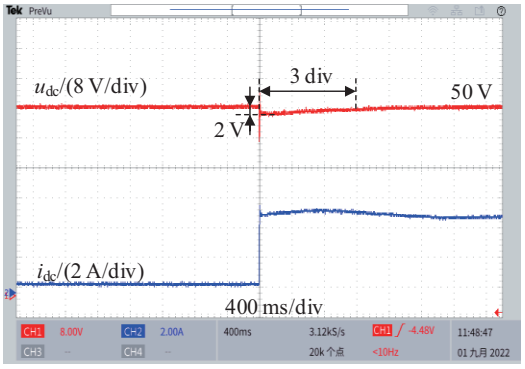

(b)

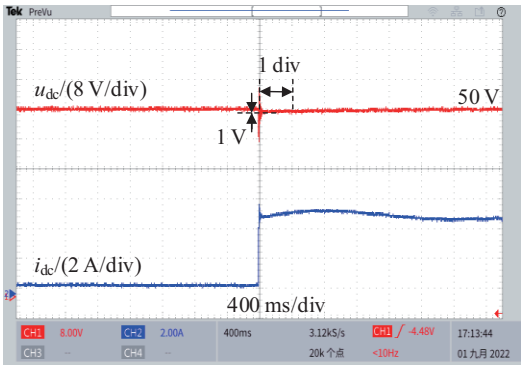

(c)

Fig. 15. Experimental waveforms of different control strategies. (a) The traditional VDMC. (b) The VDMC with armature voltage compensation. (c) The adaptive control.

V. CONCLUSION

This paper proposes a voltage compensation approach and parameter adaptive method for the VDCM of the microgrid energy storage converters. It comes out that adding armature voltage compensation can greatly suppresses the bus voltage fluctuations, but leaves the long response time issue unsolved. The dynamic characteristics and stability analysis indicate that a bigger J and k results in a decrease of maximum voltage deviation value, while lengthens the recovery time. Additionally, a bigger J can lead to an increase in overshoot. On the other hand, a bigger D will reduce the overshoot and shorten the recovery time. The adaptive parameter adaptive method can not only suppress the DC bus voltage fluctuations, but also significantly reduce the dynamic recovery time, thus enhance the stability of the DC microgrid.

References

[1] D. Dong, I. Cvetkovic, D. Boroyevich, Z. Wei, and P. Mattavelli, "Grid-interface bidirectional converter for residential DC distribution systems—Part One: high-density two-stage topology," in *IEEE Transactions on Power Electronics,* vol. 28, no. 4, pp. 1655–1666, Apr. 2013.

[2] O. Cornea, G. -D. Andreescu, N. Muntean, and H. Dan, "Bidirectional power flow control in a DC microgrid through a switched-capacitor cell hybrid DC-DC converter," in *IEEE Transactions on Industrial Electronics*, vol. 64, no. 4, pp. 3012–3022, Apr. 2017.

[3] H. Kakigano, Y . Miura, and T. Ise, "Distribution voltage control for dc microgrids using fuzzy control and gain-scheduling technique," in *IEEE Transactions on Power Electronics*, vol. 28, no. 5, pp. 2246–2258, May 2013.

[4] Y .-C. Chang and C.-M. Liaw, "Establishment of a switched-reluctance generator-based common DC microgrid system," in *IEEE Transactions on Power Electronics*, vol. 26, no. 9, pp. 2512–2527, Sept. 2011.

[5] X. Li, L. Guo, S. Zhang, C. Wang, Y. W. Li, A. Chen, and Y. Feng, "Observer-based DC voltage droop and current feed-forward control of a DC microgrid," in *IEEE Transactions on Smart Grid*, vol. 9, no. 5, pp. 5207–5216, Sept. 2018.

[6] D. Kumar, F. Zare, and A. Ghosh, "DC microgrid technology: system architectures, AC grid interfaces, grounding schemes, power quality, communication networks, applications, and standardizations aspects," in *IEEE Access*, vol. 5, pp. 12230–12256, 2017.

[7] D. Das, M. J. Hossain, S. Mishra, and B. Singh, "Bidirectional power sharing of modular DABs to improve voltage stability in DC microgrids," in *IEEE Transactions on Industry Applications*, vol. 58, no. 2, pp. 2369–2377, Mar.-Apr. 2022.

[8] P. J. d. S. Neto, T. A. d. S. Barros, J. P. C. Silveira, E. R. Filho, and J. M. Guerrero, "Power management strategy based on virtual inertia for DC microgrids," in *IEEE Transactions on Power Electronics*, vol. 35, no. 11, pp. 12472–12485, Nov. 2020.

[9] S. Samanta, J. P. Mishra, and B. K. Roy, "Virtual DC machine: An inertia emulation and control technique for a bidirectional DC-DC converter in a DC microgrid," in *IET Electric Power Applications*, vol. 12, no. 6, pp. 874–884, Jul. 2018.

[10] M. Su, Z. Liu, Y. Sun, H. Han, and X. Hou, "Stability analysis and stabilization methods of DC microgrid with multiple parallel-connected DC–DC converters loaded by CPLs," in *IEEE Transactions on Smart Grid*, vol. 9, no. 1, pp. 132–142, Jan. 2018.

[11] P. Li, "Reduced-order modeling and comparative dynamic analysis of DC voltage control in DC microgrids under different droop methods," in *IEEE Transactions on Energy Conversion*, vol. 36, no. 4, pp. 3317–3333, Dec. 2021.

[12] T. Dragičević, X. Lu, J. C. Vasquez, and J. M. Guerrero, "DC microgrids–Part I: A review of control strategies and stabilization techniques," in *IEEE Transactions on Power Electronics,* vol. 31, no. 7, pp. 4876–4891, Jul. 2016.

[13] M. Mao, Q. Cheng, and Y. Ding, "Decentralized coordination power control for islanding microgrid based on PV/BES-VSG," in *CPSS Transactions on Power Electronics and Applications*, vol. 3, no. 1, pp.14–24, Mar. 2018.

[14] C. Zhong, J. Zhang, and Y. Zhou, "Adaptive virtual capacitor control for MTDC system with deloaded wind power plants," in *IEEE Access*, vol. 8, pp. 190582–190595, 2020.

[15] Q. Peng, J. Fang, Y. Yang, T. Liu, and F. Blaabjerg, "Maximum virtual inertia from DC-Link capacitors considering system stability at voltage control timescale," in *IEEE Journal on Emerging and Selected Topics in Circuits and Systems*, vol. 11, no. 1, pp. 79–89, Mar. 2021.

[16] N. Zhi, K. Ding, L. Du, and H. Zhang, "An SOC-based virtual DC machine control for distributed storage systems in DC microgrids," in *IEEE Transactions on Energy Conversion*, vol. 35, no. 3, pp. 1411–1420, 2020.

[17] S. Samanta, J. P. Mishra, and B. K. Roy, "Virtual DC machine: An inertia emulation and control technique for a bidirectional DC-DC converter in a DC microgrid," in *IET Electric Power Applications*, vol. 12, no. 6, pp. 874–884, 2018.

[18] D. Chen, Y. Xu, and A. Huan, "Integration of DC microgrids as virtual synchronous machines into the AC grid," in *IEEE Transactions on Industrial Electronics*, vol. 64, no. 9, pp. 7455–7466, 2017.

[19] W. Sheng, H. Liu, Z. Zeng, Z. Lü, and L. Ran, "An energy hub based on virtual-machine control," in *Zhongguo Dianji Gongcheng Xuebao/ Proceedings*, vol. 35, no. 14, pp. 3541–3550, 2015.

[20] Y. Cao, W. Wang, Y. Li, Y. Tan, C. Chen, L. He, U. Haeger, and C. Rehtanz, "A virtual synchronous generator control strategy for VSC-MTDC systems," in *IEEE Transactions on Energy Conversion*, vol. 33, no. 2, pp. 750–761, Jun. 2018.

[21] E. Hammad, A. Farraj, and D. Kundur, "On effective virtual inertia of storage-based distributed control for transient stability," in *IEEE Transactions on Smart Grid*, vol. 10, no. 1, pp. 327–336, Jan. 2019.

[22] P. Wang, J. Zhao, and K. Liu, "Parameter-adaptation-based virtual DC motor control method for energy storage converter," in *IEEE Access*, vol. 9, pp. 90795–90804, 2021.

[23] G. Lin, J. Ma, Y. Li, C. Rehtanz, J. Liu, Z. Wang, P. Wang, and F. She, "A virtual inertia and damping control to suppress voltage oscillation in islanded DC microgrid," in *IEEE Transactions on Energy Conversion,* vol. 36, no. 3, pp. 1711–1721, Sept. 2021.

[24] X. Zhu and Y. Zhang, "Control strategy of DC microgrid under unbalanced grid voltage," in *Proceedings of 2016 IPEMC-ECCE Asia*, Hefei, 2016, pp. 1725–1731.

Hailiang Xu received the B.S. and Ph.D. degrees both in electrical engineering from China University of Petroleum (East China), Qingdao, China, and Zhejiang University, Hangzhou, China, in 2008 and 2014, respectively. He is currently working as a Professor with the New Energy College, China University of Petroleum (East China), Qingdao, China. His current research interests include renewable energy generation and microgrid.

Honglong Zhang received the B.S. degree from the China University of Petroleum (East China), Qingdao, China, in 2022. He is currently pursuing the master's degree with the New Energy College, China University of Petroleum (East China), Qingdao, China. His current research interests include stability analysis and control of DC microgrid.

Pingjuan Ge received the B.S. and Ph.D. degrees both in electrical engineering from Anhui University, Hefei, China, and Hunan University, Changsha, China, in 2017 and 2022, respectively. She is currently working as a Lecture with the New Energy College, China University of Petroleum (East China), Qingdao, China. Her current research interests include modeling and transient stability analysis of the power-electronic-based power systems.

Cong Wang received the B.S. degree from the Shandong University of Science and Technology in 2022. She is currently pursuing the master's degree with the New Energy College, China University of Petroleum (East China), Qingdao, China. Her current research interests include transient stability analysis of grid-connected inverters.